Spectrochimica Acta Part A: Molecular and Biomolecular Spectroscopy 105 (2013) 600–611

Contents lists available at SciVerse ScienceDirect

Spectrochimica Acta Part A: Molecular and Biomolecular Spectroscopy

journal homepage: www.elsevier.com/locate/saa

Preparation, spectroscopic investigation and antiproliferative capacity of new metal complexes of (3E)-2-(hydroxyimino)-N-P-Tolyl-3-(P-tolylimino) butanamide

Abdou Saad El-Tabl [a,*], Moshira Mohamed Abd El-wahed [b], Samar Ebrahim Abd El-Razek [a]

[a] Chemistry Department, Faculty of Science, Menoufia University, Shebin El-Kom, Egypt
[b] Pathology Department, Faculty of Medicine, Menoufia University, Shebin El-Kom, Egypt

HIGHLIGHTS

- Preparation of ligand.
- Preparation of complexes.
- Characterization of complexes using Physical techniques, Elemental analyses, Spectral technique, Thermal technique.
- Antiproliferative capacity.

GRAPHICAL ABSTRACT

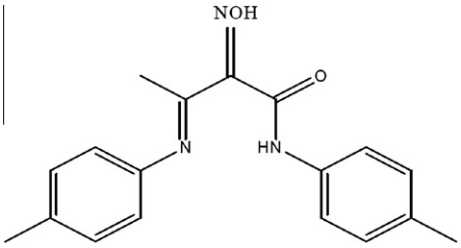

ARTICLE INFO

Article history:
Received 26 September 2012
Received in revised form 8 November 2012
Accepted 16 November 2012
Available online 23 December 2012

Keywords:
Complexes
Spectral and magnetic measurments,
Antiproliferative capacity

ABSTRACT

Cr(III), Mn(II), Fe(III), Co(II), Ni(II), Cu(II), Zn(II), Cd(II), Sr(II), Hg(II), Tl(I), UO_2(II) and ZrO(II) complexes of (3E)-2-(hydroxyimino)-N-P-Tolyl-3-(P-tolylimino) butanamide have been prepared and characterized by elemental analyses, IR, UV–Vis spectra, magnetic moments, conductances, ^{1}H NMR and mass spectra (ligand and its Zn(II) complex), thermal analyses (DTA and TGA) and ESR measurements. The IR data show that, the ligand behaves as monobasic bidentate or neutral bidentate. Molar conductances in DMF indicate that, the complexes are non-electrolytes. ESR spectra of solid Cu(II) complexes at room temperature show axial type (d_{x2-y2}) with covalent bond character in an octahedral environment. Complexes showed inhibitory activity against hepatocellular carcinoma (HepG-2 cell line).

Introduction

Recently, considerable attention has been given to oximes and their coordination complexes due to their biological activities as fungicides [1,2] bactericides [1–3], analgesic, anti-inflammatory [4], antioxidant [1] and antitumor [5–7]. Also, oximes and their complexes have applications in medicine, bioorganic systems, catalysis, electrochemical, electro-optical sensors, semiconducting properties and as model compounds [8–11]. Oximes formed mixed ligands with pyridine, imidazol etc., that are very similar to those found in nature [12]. The bioactivity of oximes was related to the coordination mode of the oxime site (N and O coordination modes) [13,14] as well as to the bridging capacity of the coordinated oximato group to metal ions [15,16]. The bridging oxygen atom of the oximato group serves as a binding site for developing supermolecular structures [17]. Oximes have been used in analytical chemistry for isolation, separation and extraction of different metal ions [18,19]. Complexes $[Ni(HL^1)_2](ClO_4)_2$, $[Ni(HL^2)_2](ClO_4)_2$ and $[Ni(HL^3)]ClO_4$ have been prepared and spectrally characterized [20], where [HL^1 = 3-(2-amino-ethylimino)-butan-2-one oxime, HL^2 = 3-(2-amino-propylimino)-butan-2-one oxime] and HL^3 = 3-[2-(3-hydroxy-1-methyl-butan-2-enylideneamino)-1-methyl-ethylimino)-butan-2-one oxime. Copper(II) complexes of N,N-diacetyloximo-1,3-phenylenediamine have been prepared and spectrally characterized [21]. This paper describes the synthesis of a new ligand and its complexes and to investigate the ESR and spectral data associated with the resulting structures. This approach is of

* Corresponding author.
E-mail address: asaeltabl@yahoo.com (A.S. El-Tabl).

1386-1425/$ - see front matter © 2012 Published by Elsevier B.V.
http://dx.doi.org/10.1016/j.saa.2012.11.056

fundamental importance to the structural estimation of the other metal complexes and to the metal binding sites of various metalloenzymes [22].

Experimental

Materials

All the reagents were of the best grade available and used without further purification.

Physical measurements

C, H, N and Cl analyses were determined at the Analytical Unit of Cairo University, Egypt. A standard method [gravimetric] was used to determine metal(II)/(III) ions [23]. All complexes were dried under vacuum over P_4O_{10}. The IR spectra were measured as KBr and CeBr pellets using a Perkin-Elmer 683 spectrophotometer (4000–200 cm^{-1}). Electronic spectra were recorded on a Perkin–Elmer 550 spectrophotometer. The conductance of (10^{-3} M DMF) of the complexes were measured at 25 °C with a Bibby conductimeter type MCl. ^1H NMR spectra (ligand and its Zn(II) complex) were obtained with Perkin–Elmer R32-90-MHz spectrophotometer using TMS as internal standard. Mass spectra (ligand and its Zn(II) complex) were recorded using JEULJMS-AX-500 mass spectrometer provided with data system. The thermal analyses (DTA and TGA) were carried out in air on a Shimadzu DT-30 thermal analyzer from 27 to 800 °C at a heating rate of 10 °C per minute. Magnetic susceptibilities were measured at 25 °C by the Gouy method using mercuric tetrathiocyanato cobalt(II) as the magnetic susceptibility standard. Diamagnetic corrections were estimated from Pascal's constant [24]. The magnetic moments were calculated from the equation: $\mu_{eff} = 2.84\sqrt{\chi_m^{corr}.T}$. The ESR spectra of solid complexes at room temperature were recorded using a varian E-109 spectrophotometer, DPPH was used as a standard material. The T.L.C of the ligand and its complexes confirmed their purity.

Preparation of the ligand and its metal complexes

Preparation of the ligand, [HL] (*1*)

Ligand **(1)** was prepared by refluxing with stiring equimolar amounts of oxime (10 g, 0.0628 mol) and para-toludine (6.72 g, 0.0628 mol) in ethanol (100 cm^3) for 2 h. The pale yellow product obtained was filtered off, washed several times with ethanol and dried in vacuum over P_4O_{10}. Analytical data are given in Table 1.

Synthesis of metal complexes (*2*)–(*20*)

A filtered ethanolic (100 cm^3) of $Cu(OAc)_2{\cdot}H_2O$ (4.02 g, 0.0201 mol) was added to an ethanolic (100 cm^3) of the ligand, **(1)** (5.0 g, 0.0201 mol) [1L:1M], complex **(2)**, (8.04 g, 0.0402 mol) of $Cu(OAc)_2{\cdot}H_2O$ [1L:2M], complex **(3)**, (2.01 g, 0.01 mol) of $Cu(OAc)_2{\cdot}H_2O$ [2L:1M] complex **(4)**, (3.21 g, 0.0201 mol) of $CuSO_4$ complex **(5)**, (2.71 g, 0.0201 mol) of $CuCl_2$ complex **(6)**, (4.87 g, 0.0201 mol) of $Cu(NO_3)_2{\cdot}3H_2O$ complex **(7)**, (5.01 g, 0.0201 mol) of $Ni(OAc)_2{\cdot}4H_2O$ complex **(8)**, (3.12 g, 0.0201 mol) of $CoSO_4{\cdot}H_2O$ complex **(9)**, (4.94 g, 0.0201 mol) of $Mn(OAc)_2{\cdot}4H_2O$ complex **(10)**, (4.42 g, 0.0201 mol) of $Zn(OAc)_2{\cdot}2H_2O$ complex **(11)**, (8.55 g, 0.0201 mol) of $UO_2(OAc)_2$ complex **(12)**, (6.42 g, 0.0201 mol) 0f $Hg(OAc)_2$ complex **(13)**, (5.31 g, 0.0201 mol) of Tl(OAc) complex **(14)**, (5.44 g, 0.0201 mol) of $FeCl_3{\cdot}6H_2O$ complex **(15)**, (5.37 g, 0.0201 mol) of $CrCl_3{\cdot}6H_2O$ complex **(16)**, (6.49 g, 0.0201 mol) of $ZrOCl_2{\cdot}8H_2O$ complex **(17)**, (5.37 g, 0.0201 mol) of $SrCl_3{\cdot}6H_2O$ complex **(18)**, (5.37 g, 0.0201 mol) of $Cd(OAc)_2{\cdot}H_2O$ complex **(19)**, (5.17 g, 0.0201 mol) of $CdSO_4$ complex **(20)**. All complexes were prepared using 3 ml DMA except complexes **(2)**, **(3)**, **(4)**, **(8)** and **(10).** The mixture was refluxed with stirring for 1–3 h, depending on the nature of metal salts, the colored complex was filtered off, washed with ethanol and dried under vacuo over P_4O_{10}.

Biological evaluation

The antiproliferative activity was measured invitro for the synthesized complexes according to Sulfo-Rhodamine-B-stain (SRB) assay using the published methods [25]. Cells were plated in 96-multiwell plate (10^4 cells/well) for 24 h before treatment with the complexes to allow attachment of cell to the wall of the plate. Different concentration of the compound in DMSO (1.56, 3.125, 6.25, 12.5, 25 and 50 μg/ml) was added to the cell monolayer triplicate. Monolayer cells were incubated with the complexes for 48 h at 37 °C under atmosphere of 5% CO_2. After 48 h, cells were fixed, washed and stained with Sulfo-Rhodamine-B-stain. Excess stain was wash with acetic acid and attached stain was recovered with Tris EDTA buffer (10 m M TrisHCl + 1 m M Disodium EDTA, pH 7.5–8). Color intensity was measured by ELISA reader. The relation between surviving fraction and drug concentration is plotted to get the survival curve of each tumor cell line after the specified complex. Sorafenib is used as a standard drug.

Results and discussion

All the complexes are stable at room temperature, non hydroscopic, insoluble in water and partially soluble in common organic solvents such as $CHCl_3$, but soluble in DMF and DMSO. The analytical and physical data of the ligand and its complexes are given in Table 1, spectral data Tables 2–5 are compatible with the proposed structures, Fig. 1. The molar conductances are in the (22–11) $ohm^{-1}\ cm^2\ mol^{-1}$ range, Table 1, indicating a non-electrolytic nature [26]. The high value for some complexes suggests partial dissociation in DMF. Many attempts were made to grow a single crystal but unfortunately, they were failed. Reaction of **(1)** with metal salts using (1L:1M), (1L:2M) and (2L:1M) molar ratios in ethanol gives complexes **(2)–(20).** The composition of the complexes formed depends on metal salts, the medium of the reaction and the molar ratios.

^1H NMR spectra

The ^1H NMR spectra of the ligand and its Zn(II) complex **(11)** in deuterated DMSO show signals consistent with the proposed structure. Ligand shows peaks at 7.59 and 7.34 ppm, are assigned to protons of NH group [27–29]. The signal of oxime group is observed at 9.6 ppm [29–31]. The lower the value, may be due to hydrogen bonding of the oxime group. Resonances appeared in the 4.0–4.18 and 2.5–2.17 ppm ranges are due to methyl attach to imino group and methyl group attach to phenyl group respectively [27,29,32]. Also, the spectrum showed a set of peaks as multiples at 6.65–7.33 ppm range which are assigned to the protons of aromatic ring [2]. However, for Zn(II) complex **(11),** the signal due to the oxime proton is disappeared, indicating coordination to the Zn(II) ion. The signals observed at 7.42 and 7.12 ppm are assigned to —NH proton [2]. A set of peaks appeared as multiples at 6.25–7.28 ppm range are corresponding to protons of aromatic ring [2]. The signals appeared at 3.48 and 2.79–2.32 ppm range are due to methyl attach to imino group and the methyl attach to the phenyl group [2]. The appearance of new signal at 1.88 ppm is due to protons of coordinated acetate group [33,34].

Table 1
Analytical and physical data of the ligand [HL], (1) and its metal complexes.

No.	Ligands/complexes	Color	FW	M.P. (°C)	Yield (%)	Anal./Found (Calc.) (%)				Molar conductance $\Lambda m(\Omega^{-1}\,cm^2\,mol^{-1})$
						C	H	N	M	
(1)	[HL] $C_{18}H_{19}N_3O_2$	Pale yellow	309	191	75	69.92 (69.99)	6.22 (6.14)	13.34 (13.59)	–	–
(2)	$[LCu(OAc)(H2O)3]\cdot H_2O$ $C_{20}H_{29}N_3O_8Cu$	Dark green	502.5	>300	80	47.5 (47.76)	5.31 (5.77)	7.91 (8.35)	11.98 (12.63)	12
(3)	$[L(Cu)_2(OAc)_3(H_2O)_5]\cdot 3H_2O$ $C_{24}H_{43}N_3O_{16}Cu_2$	Dark green	756	>300	84	38.72 (38.09)	5.33 (5.68)	5.21 (5.55)	16.32 (16.79)	14
(4)	$[(L)_2Cu(H_2O)_2]\cdot H_2O$ $C_{36}H_{42}N_6O_7Cu$	Green	733.5	>300	72	58.86 (58.89)	5.21 (5.72)	11.1 (11.45)	8.41 (8.65)	13
(5)	$[(HL)Cu(SO_4)(H_2O)_3]\cdot 5H_2O$ $C_{18}H_{39}N_3O_{14}SCu$	Pale green	636.5	260	69	33.35 (33.93)	5.95 (6.12)	6.91 (6.59)	10.1 (9.97)	14
(6)	$[LCu(Cl)(H_2O)_3]\cdot 2H_2O$ $C_{18}H_{28}N_3O_7ClCu$	Pale green	496.9	>300	71	42.96 (43.46)	5.16 (5.63)	8.2 (8.45)	12.54 (12.77)	15
(7)	$[LCu(NO_3)(H_2O)_3]\cdot 3H_2O$ $C_{18}H_{30}N_4O_{11}Cu$	Dark green	541.5	>300	80	39.8 (39.88)	5.26 (5.54)	9.91 (10.34)	11.21 (11.72)	16
(8)	$[LNi(OAc)(H_2O)_3]\cdot 3H_2O$ $C_{20}H_{33}N_3O_{10}Ni$	Pale green	533.6	196	72	44.49 (44.97)	5.69 (6.18)	7.23 (7.87)	10.45 (10.98)	14
(9)	$[HLCo(SO_4)(H_2O)_3]\cdot 2H_2O$ $C_{18}H_{33}\ N_3O_{11}SCo$	Brown	557.9	>300	68	38.06 (38.71)	5.19 (5.91)	7.22 (7.52)	10.11 (10.55)	12
(10)	$[LMn(OAc)(H_2O)_3]\cdot H_2O$ $C_{20}H_{29}N_3O_8Mn$	Dark brown	493.9	250	65	48.3 (48.59)	6.01 (5.87)	8.12 (8.5)	11.07 (11.11)	13
(11)	$[LZn(OAc)(H_2O)_3]\cdot 3H_2O$ $C_{20}H_{33}N_3O_{10}Zn$	Pale brown	540.39	>300	65	44.8 (44.41)	5.9 (6.1)	7.81 (7.77)	12.4 (12.1)	18
(12)	$[LUO_2(OAc)(H_2O)_3]\cdot H_2O$ $C_{20}H_{29}N_3O_8UO_2$	Yellow	677	>300	89	35.1 (35.45)	4.0 (4.28)	6.0 (6.2)	35.9 (35.15)	11
(13)	$[HLHg(OAc)_2]\cdot H_2O$ $C_{22}H_{27}N_3O_7Hg$	Dark green	645.59	270	55	39.9 (40.89)	4.32 (4.18)	6.4 (6.5)	29.87 (30.07)	14
(14)	$[HLTl(OAc)(H_2O)_3]\cdot H_2O$ $C_{20}H_{30}N_3O_8Tl$	Pale white	644.38	>300	82	37.13 (37.24)	4.51 (4.65)	6.5 (6.51)	31.01 (31.71)	19
(15)	$[LFe(Cl)_2(H_2O)_2]\cdot 3H_2O$ $C_{18}H_{28}N_3O_7Cl_2Fe$	Dark brown	524.6	205	74	40.98 (41.17)	5.32 (5.33)	8.1 (8.0)	10.41 (10.63)	20
(16)	$[LCr(Cl)_2(H_2O)_2]\cdot 3H_2O$ $C_{18}H_{28}N_3O_7Cl_2Cr$	Dark green	520.7	165	66	41.22 (41.48)	5.51 (5.37)	8.11 (8.06)	9.81 (9.96)	22
(17)	$[LZrO(Cl)_2(H_2O)]\cdot H_2O$ $C_{18}H_{22}N_3O_5Cl_2Zr$	Pale yellow	522	>300	73	41.01 (41.37)	4.71 (4.21)	8.0 (8.04)	17.92 (17.47)	21
(18)	$[HLSr(Cl)_2(H_2O)_2]\cdot 2H_2O$ $C_{18}H_{27}N_3O_6Cl_2Sr$	Pale yellow	539.42	>300	76	39.9 (40.04)	5.12 (5.005)	7.65 (7.78)	15.93 (16.24)	21
(19)	$[LCd(OAc)(H_2O)_3]\cdot 2H_2O$ $C_{20}H_{31}N_3O_9Cd$	White	569.41	>300	70	41.9 (42.14)	5.04 (5.44)	7.03 (7.37)	19.22 (19.66)	17
(20)	$[HLCd(SO_4)(H_2O)_3]\cdot 2H_2O$ $C_{18}H_{29}N_3O_{11}SCd$	White	607.41	>300	66	35.0 (35.56)	5.0 (4.77)	6.23 (6.91)	17.9 (18.5)	16

Mass spectra

The mass spectra of the ligand and its Zn(II) complex **(11)** confirmed their proposed formulations as shown in Table 6. The spectrum of ligand reveals the molecular ion peaks (m/z) at 309 amu consistent with the molecular weight of the ligand (309). Furthermore, the fragments observed at m/z = 70, 83, 86, 130, 168, 189, 203, 216, 240, 277 and 309 correspond to C_3H_4NO, C_3HNO_2, $C_3H_4NO_2$, $C_4H_8N_3O_2$, $C_{10}H_4N_2O$, $C_{10}H_9N_2O_2$, $C_{10}H_9N_3O_2$, $C_{11}H_{10}N_3O_2$, $C_{13}H_{10}N_3O_2$, $C_{14}H_{11}N_3O_2$ and $C_{18}H_{19}N_3O_2$ moiety respectively. However, the Zn(II) complex **(11)** shows peak (m/z) at 540.39 amu. Additionally, the peaks observed at 76, 104, 148, 214, 318 and 433 are due to C_6H_4, C_7H_5O, $C_7H_4N_2O_2$, $C_7H_5N_2O_2Zn$, $C_{14}H_{11}N_3O_2Zn$ and $C_{20}H_{22}N_3O_2Zn$ moieties respectively.

IR spectra

The IR spectra of the ligand and its complexes **(2)–(20)** are given in Table 2. The spectrum of **(1)** showed ν(OH) band of the oxime group at 3400 cm^{-1}, the appearance of two broad bands at 3060–3650 and 2450–3000 cm^{-1} ranges, commensurate the presence of two types of intra-and intermolecular hydrogen-bonded oxime group [21,35]. Thus, the higher frequency band is associated with a weaker hydrogen bond and the lower frequency band with a strong hydrogen bond. Also, the spectrum shows bands at 3200, 1665, 1620, and 1610 cm^{-1}, assigned to ν(NH), ν(C=O), $\nu(C{=}N)_{imine}$ and $\nu(C{=}N)_{oxime}$ respectively [31,36,37]. Medium bands at 1120, 1025 and 950 cm^{-1} are assigned to ν(NO) vibration [29,31,38]. P-substituted aromatic ring appears at 1605 and 750 cm^{-1} [39]. The IR spectra of the complexes show, the $\nu(C{=}N)_{imine}$ stretching frequency undergoes a shift to lower frequency by 9–19 cm^{-1}. This is indicative of nitrogen coordination of the azomethine to the metal ion [40,41]. The ν(C=O) of amide group appears in the 1646–1678 cm^{-1}, range. This vibration is located in the region of non-coordinated carbonyl group attached to a five-membered chelate ring [40,42]. The ν(NH) appears in the 3200–3426 cm^{-1} range [27,43]. The bands observed in the 1540–1610 cm^{-1} and 1540–1604 and 725–775 cm^{-1} ranges are

Table 2
IR frequencies of the bands (cm^{-1}) of ligand [HL] and its metal complexes and their assignments.

No.	((OH)/)H $_2$O	ν(H-bonding)	ν(NH)	ν(C=O)	ν(C=N)	ν(C=NO)	ν(Ar)	ν(NO)	υ(OAc)/SO_4/[NO_3]	υ(M—O)	υ(M—N)	υ (M—Cl)
(1)	3400	3650–3060 3000–2450	3200	1665	1620	1610	1605, 750	1120, 1025, 950	–	–	–	–
(2)	3600–3320 3300–3060	3590–3280 3300–2350	3255	1655	1610	1585	1604, 735	1160, 1110, 1025, 910	(1510, 1395)	525	460	–
(3)	3570–3300 3280–3032	3650–3290 3285–2860	32,483,228	1646	1608	1595	1565, 730	1166, 1109, 1024	(1555, 1515, 1442, 1380)	537	487	–
(4)	3620–3310 3280–3050	3580–3262 3250–2980	3250	1672	1607	1585	1565, 735	1172, 1125, 985	–	550	575, 485	–
(5)	(3370) 3516–3196 3145–3022	3630–3213 3195–2865	3231	1650	1601	1598	1590, 730	1165, 1109, 1025, 954	1109, 1037, 819, 648, 400	585	489	–
(6)	3785–3230 3165–3030	3640–3160 3080–2710	3274	1654	1608	1572	1560, 725	1106, 1065, 1047	–	508	484	426
(7)	3650–3320 3195–2900	3650–3230 3165–2700	3426	1678	1607	1590	1560, 738	1176, 1106	[1384, 1286, 819, 767]	526	432	–
(8)	3614–3259 3160–3056	3641–3179 3114–2550	3230	1655	1611	1575	1565, 738	1183, 1116, 1024, 970	(1516, 1388)	526	434	–
(9)	(3394) 3600–3275 3270–2980	3650–3200 3186–2780	3215	1653	1605	1550	1585, 737	1175, 1022, 975	1107, 1028, 807, 807, 695, 489	531	434	–
(10)	3590–3300 3290–3000	3630–3155 3119–2750	3352	1655	1610	1590	1553, 735	1121, 1072, 984	(1531, 1367)	505	466	–
(11)	3550–3260 3250–3070	3600–3250 3126–2474	3260	1665	1608	1560	1550, 750	1142, 1118, 1024	(1510, 1408)	537	478	–
(12)	3576–3337 3320–3030	3650–3300 3275–2598	3337	1670	1607	1608	1573, 735	1142, 1113, 1062	(1537, 1416)	564	479	–
(13)	(3386) 3512–3259 3232–3068	3655–3165 3125–2643	3232	1665	1605	1590	1566, 740	1184, 1111, 1026, 970	(1515, 1389)	543	468	–
(14)	(3390) 3650–2920	3620–3100 3045–2750	3266	1665	1607	1600	1540, 770	1174, 1175, 1020, 980	(1520, 1414)	587	462	–
(15)	(3426) 3634–3255 3165–2910	3595–3230 3160–2780	3230	1657	1608	1610	1572, 765	1190, 1053, 1021	–	565	480	418
(16)	3640–3250 3205–3065	3637–3110 3080–2790	3252	1665	1607	1590	1560, 745	1183, 1103, 980	–	524	446	415
(17)	3590–3270 3245–3010	3660–3190 3165–2780	3260	1670	1606	1570	1560, 730	1188, 1108, 1023, 995	–	555	460	411
(18)	(3427) 3620–3245 3214–3060	3630–3130 2985–2780	3292	1665	1605	1601	1570, 775	1194, 1144, 1023, 975	–	522	454	412
(19)	3575–3350 3335–2980	3655–3145 3080–2600	3320	1665	1607	1583	1563, 725	1183, 1106, 991	(1506, 1405)	543	462	–
(20)	(3340) 3590–3335 3300–3010	3650–3210 3124–2650	3280	1670	1608	1540	1565, 750	1188, 1105, 1023, 970	619, 450	527	431	–

Table 3
The electronic absorption spectral bands (nm) and magnetic moment (B.M.) for the ligand [HL] and its complexes.

No.	λ_{max} (nm)	μ_{eff} (B.M.)
(1)	295 nm (log ε = 4.05), 380 nm (log ε = 5.03), 400 nm (log ε = 4.29)	
(2)	290, 307, 380, 450, 530, 625	1.76
(3)	290, 310, 385, 490, 520, 615	1.53
(4)	280, 300, 380, 475, 530, 615	1.82
(5)	295, 308, 390, 456, 537, 640	1.79
(6)	285, 303, 380, 459, 532, 653	1.76
(7)	292, 310, 390, 445, 586, 645	1.65
(8)	285, 300, 385, 490, 615, 730	3.32
(9)	280, 295, 390, 530, 625	4.19
(10)	275, 300, 390, 465, 575, 630	5.29
(11)	280, 305, 400	Diam.
(12)	290, 310, 395	Diam.
(13)	265, 300, 380	Diam.
(14)	270, 305, 390, 415	2.15
(15)	265, 320, 390, 465, 590, 645	5.33
(16)	280, 305, 380, 460, 560, 635	4.40
(17)	280, 315, 400	Diam.
(18)	280, 305, 410	Diam.
(19)	285, 370, 395	Diam.
(20)	290, 365, 390	Diam.

due to $\nu(C{=}N)_{oxime}$ and aromatic groups [21,39,40]. The complexes show strong bands in the 1103–1194 and 970–1097 cm^{-1}, ranges, indicating N-coordination of the oximato group [21,40,44]. Complexes **(5)**, **(9)**, **(13)**, **(14)**, **(15)**, **(18)** and **(20)** show bands in the 1020–1194 and 954–980 cm^{-1}, ranges Table 2 corresponding to ν(NOH) [40,42]. However, complexes **(5)**, **(9)**, **(13)**, **(14)**, **(15)**, **(18)** and **(20)** show medium band in the 3340–3427 cm^{-1} range is due to ν(OH) group [21,39]. Complexes show broad bands in the 3100–3660 and 2350–3335 cm^{-1}, ranges, corresponding to intra-and intermolecular hydrogen bondings [21,35], however, the hydrated and coordinated water molecules appear in the 3196–3650 and 2900–3320 cm^{-1} ranges [27,45,46]. Extensive IR spectral studies reported on metal acetate complexes [39,47] indicate that, the acetate ligand coordinates in either a monodentate, bidentate or bridging manner, the $\nu_a(CO_2)$ and $\nu_s(CO_2)$ of the free acetate are observed at 1560 and 1416 cm^{-1} respectively. In monodentate, the coordination of ν(C═O) is observed at higher energy than $\nu_a(CO_2)$ and ν(C—O) is appeared at lower than $\nu_s(CO_2)$. As a result, the separation between (CO) bands is much larger in monodentate complexes. In complexes **(2)**, **(3)**, **(8)**, **(10)**, **(11)**, **(12)**, **(13)**, **(14)** and **(19)**, the band is due to $\nu(CO_2)$ appears in the 1506–1537 cm^{-1} and the $\nu_s(CO_2)$ observed in the 1367–1416 cm^{-1}

Table 4
ESR data for the metal (II) complexes.

No.	$g_{\|}$	$g_{\perp}$	g_{iso}[a]	$A_{\|}$ (G)	$A_{\perp}$ (G)	A_{iso}[b] (G)	G[c]	ΔE_{xy}	ΔE_{xz}	$K_{\perp}^2$	$K_{\|}^2$	K	$g_{\|}/A_{\|}$	α^2	β^2	β_1^2	-2β	a_d^2 (%)
(2)	2.10	2.02	2.04	130	15	53.3	5.0	18868	20204	0.23	0.28	0.53	165.4	0.50	0.46	0.56	157	66.7
(3)	2.12	2.06	2.08	140	25	63.3	2.0	19231	20408	0.71	0.34	0.58	151.4	0.56	1.27	0.61	160	68.1
(7)	2.16	2.03	2.07	150	30	70	2.3	17065	22472	0.38	0.41	0.64	144	0.65	0.58	0.63	173.2	74.0
(9)	–	–	2.09	–	–	–	–	–	–	–	–	–	–	–	–	–	–	–
(10)	–	–	2.12	–	–	–	–	–	–	–	–	–	–	–	–	–	–	–

[a] $g_{iso} = (2g_{\perp} + g_{\|})/3$.
[b] $A_{iso} = (2A_{\perp} + A_{\|})/3$.
[c] $G = (g_{\|} - 2)/(g_{\perp} - 2)$.

Table 5
Thermal data for the metal complexes.

No.	Temp. (°C)	DTA (Peak)	TGA (wt. loss%)		Assignment
			Calc.	Found	
(3)	60	Endo	7.14	7.34	Loss of three hydrated water
	170	Endo	10.25	10.45	Loss of four coordinated water
	255	Endo	9.36	9.79	Loss of one terminal coordinated acetate
	285	Endo	20.66	21.1	Loss of two bridge coordinated acetate
	365	Endo	–	–	Melting point
	465, 515, 595	Exo	17.55	17.66	Decomposition with formation CuO
(6)	65	Endo	7.24	7.42	Loss of two hydrated water
	145, 165	Endo	11.71	11.9	Loss of three coordinated water
	250	Endo	8.72	8.91	Loss of one Cl
	325	Endo	–	–	Melting point
	365, 390, 430, 500, 570	Exo	21.53	21.57	Decomposition with formation of CuO
(7)	80	Endo	9.93	9.63	Loss of three hydrated water
	170	Endo	11.02	11.85	Loss of three coordinated water
	255	Endo	13.90	13.33	Loss of one NO_3 group
	330	Endo	–	–	Melting point
	360, 445, 500, 540, 615	Exo	20.83	20.74	Decomposition with formation of CuO
(9)	60	Endo	6.51	6.03	Loss of two hydration water
	120	Endo	10.44	10.34	Loss of three coordinated water
	220	Endo	20.73	21.36	Loss of SO_4
	257	Endo	47.41	47.41	Loss of two (C_7H_7)
	316	Endo	–	–	Melting point
	400, 480, 595	Exo	38.34	38.79	Thermal decomposition with the formation of CoO
(11)	64	Endo	9.3	9.02	Loss of three hydrated water
	125, 161	Endo	10.24	10.52	Loss of three coordinated water
	294	Endo	12.46	12.46	Loss of acetate group
	332	Endo	–	–	Melting point
	416, 550, 600	Exo	19.54	19.1	Decomposition with formation of ZnO

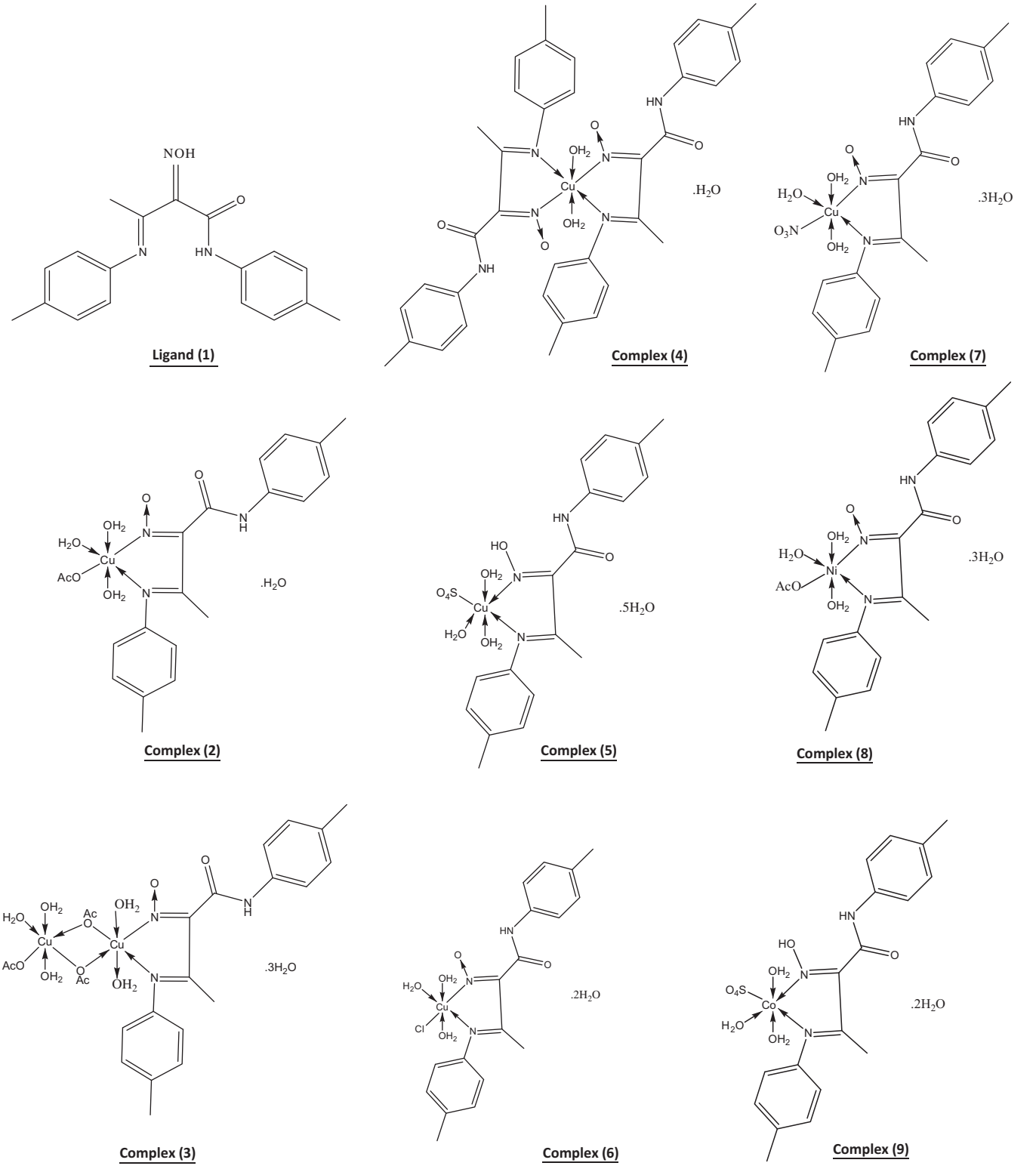

Fig. 1. Structures of complexes.

ranges. The difference between these two bands is in the 101–164 cm^{-1} range, suggesting that, the acetate group coordinates in unidentate manner with the metal ion [39,47,48]. However, bridging acetate with both oxygen atoms coordinated have ν(CO) bands close to the free ion values [39,47,48] as found for complex **(3),** $\nu_a(CO_2)$ = 1555 and $\nu_s(CO_2)$ = 1422 cm^{-1}. Complexes **(5)**, **(9)** and **(20)** show bands at 1109, 1037, 819, 648 and 441, 1107, 1028, 807, 695 and 489 and 1112, 1030, 809, 619 and 450 cm^{-1} respectively are corresponding to monodentate coordinate sulfate group [49]. Complexes **(6)**, **(15)–(18)** show bands at 426, 418, 415, 411 and 412 cm^{-1} respectively, assigned to ν(M—Cl) [50]. Complex **(7)** shows bands at 1384, 1286, 819 and 767 cm^{-1}, assigned to coordinated nitrate group [51,52]. Complex **(12)** shows a band at 900 cm^{-1} is due to O=U=O [53], however, complex **(17)** shows a

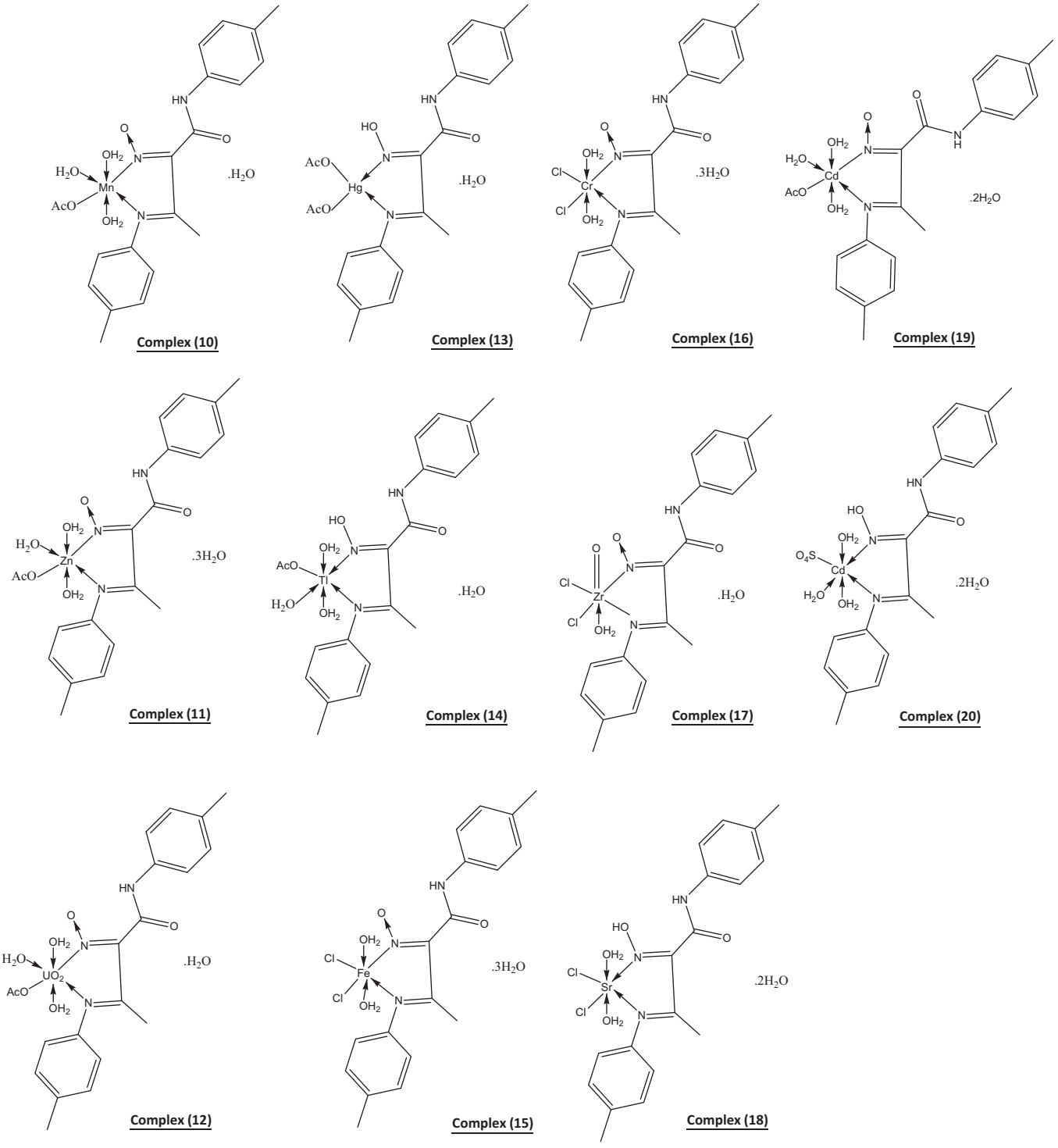

Fig. 1. (*continued*)

band at 841 cm^{-1}, assigned to (ZrO) vibration [54]. The bonding of the metal ions to the ligand through the oxygen and nitrogen atoms is further supported by the presence of new bands in the 505–587 and 431–489 cm^{-1} ranges respectively [27,40,50].

Magnetic moments

The magnetic moments of the complexes **(2)–(20)** are shown in Table 3. Copper(II) complexes **(2)–(7)** show values 1.53–1.82 B.M. range, corresponding to one unpaired electron in an octahedral structure [47,50], complexes **(3)** and **(7)** show values which are well below the spin only value (1.73 B.M.), indicating that, spin-exchange interactions takeplace between the copper(II) ion through acetate group, or hydrogen bonding in an octahedral geometry [55]. Nickel(II) complex **(8)** shows a value 3.32 B.M., indicating an octahedral geometry around Ni(II) ion [56]. Cobalt(II) complex **(9)** shows 4.19 B.M., indicating high spin octahedral cobalt(II) complexes [27,57]. Manganese(II) complex **(10)** shows 5.29 B.M., suggesting high spin octahedral geometry around the Mn(II) ion [27,57]. Thalium(I) complex **(14)** gave 2.15 B.M., indicating octahe-

dral Tl(I) complex [58]. Iron(III) complex **(15)** and chromium(III) complex **(16)** show values 5.33 and 4.4 B.M., indicating high spin octahedral structure [57]. Zinc(II), complex **(11)**, uranyl(II) complex **(12)**, mercury(II) complex **(13)**, zironyl(II) complex **(17)**, strontium(II) complex **(18)**, cadmium(II) complexes **(19)** and **(20)** show diamagnetic property [21].

Electronic spectra

The electronic spectral data for the ligand and its complexes in DMF solution are summarized in Table 3. Ligand in DMF solution shows three bands at 400 nm ($\log \varepsilon = 4.29$), 380 nm ($\log \varepsilon = 5.03$) and 295 nm ($\log \varepsilon = 4.05$), which may be assigned to the $n \rightarrow \pi^*$ and $\pi \rightarrow \pi^*$ transitions respectively [59]. Copper(II) complexes **(2)–(7)** show bands in the 295–280, 310–300 and 390–380 nm ranges, these bands are due to intraligand transitions, however, the bands appear in the 490–445, 586–520 and 653–615 nm ranges are assigned to O → Cu charge transfer, $^2B_1 \rightarrow {}^2E$ and $^2B_1 \rightarrow {}^2B_2$ transitions, indicating a distorted tetragonal octahedral structure [60–62]. Nickel(II) complex **(8)** shows bands 285, 300, 385, 490, 615 and 730 nm respectively, the first three bands are within the ligand and the other three bands are attributable to $^3A_{2g}(F) \rightarrow {}^3T_{1g}(P)(\nu_3)$, $^3A_{2g}(F) \rightarrow {}^3T_{1g}(F)(\nu_2)$ and $^3A_{2g}(F) \rightarrow {}^3T_{2g}(F)(\nu_1)$ transitions respectively, indicating an octahedral Ni(II) complex [60,63]. The ν_2/ν_1 ratio for the complex is 1.19, which is less than the usual range of 1.5–1.75, indicating a distorted octahedral Ni(II) complex [60,64]. Cobalt(II) complex **(9)** shows bands at 280, 295, 390, 530 and 625 nm, the first three bands are within the ligand and the other bands are assigned to $^4T_{1g}(F) \rightarrow {}^4A_{2g}$ and $^4T_{1g}(F) \rightarrow {}^4T_{2g}(F)$ transitions respectively, corresponding to high spin Co(II) octahedral complexes [65]. Manganese(II) complex **(10)** shows bands at 275, 300, 390, 465, 575 and 630 nm, respectively, the first three bands are within the ligand, however, the other bands are corresponding to $^6A_{1g} \rightarrow {}^4E_g$, $^6A_{1g} \rightarrow {}^4T_{2g}$ and $^6A_{1g} \rightarrow {}^4T_{1g}$ transitions which are compatible to an octahedral geometry around the Mn(II) ion [66]. Tl(I) complex **(14)** gave bands at 270, 305 and 390 nm, respectively. These bands are due to intraligand transitions since these bands appear almost in the spectrum of the ligand, additional weak band appears at 415 nm, which may be assigned to the $^1S_0 \rightarrow {}^3P_1$ transition of Tl(I) complex [67]. Iron(III) complex **(15)** shows bands at 265, 320, 390,465, 590 and 645 nm respectively, the first three bands are within the ligand while the other bands are due to charge transfer and $^6A_1 \rightarrow {}^4T_1$ transitions, suggesting distorted octahedral geometry around the iron(III) ion [68,69]. While chromium(III) complex **(16)** shows bands at 280, 305, 380, 460, 560 and 635 nm respectively. The first three bands are within the ligand and the other bands are assigned to $^4A_{2g} \rightarrow {}^4T_{1g}(F)$, $^4A_{2g} \rightarrow {}^4T_{2g}$ and $^4A_{2g} \rightarrow {}^2T_{2g}$ transitions respectively, indicating octahedral structure around the Cr(III) ion [70,71]. Zinc(II) complex **(11)**, uranyl(II) complex **(12)**, mercury(II) complex **(13)**, zirconyl(II) complex **(17)**, strontium(II) complex **(18)** and cadmium(II) complexes **(19)** and **(20)** show three bands in the 290–265, 370–300 and 415–380 nm ranges, which are assigned to intraligand transitions.

Electron spin resonance (ESR)

The ESR spectral data for complexes **(2)**, **(3)**, **(7)**, **(9)** and **(10)** are presented in Table 4. The spectra of copper(II) complexes **(2)**, **(3)** and **(7)** are characteristic of species, d^9 configuration and having axial type of a $d_{(x2-y2)}$ ground state which is the most common for copper(II) complexes [72,73]. The complexes show $g_{||} > g_{\perp} > 2.0023$, indicating octahedral geometry around copper(II) ion [74,75]. The g-values are related by the expression [74,76], $G = (g_{||} - 2)/(g_{\perp} - 2)$, if $G > 4.0$, then, local tetragonal axes are aligned parallel or only slightly misaligned, if $G < 4.0$, the significant exchange coupling is present. Complexes **(3)** and **(7)** show values 2.0 and 2.3 indicating spin–exchange interactions takeplace between copper(II) ions through acetate group **(3)** or hydrogen bondings **(7)**. This phenomenon is further confirmed by magnetic moments (1.53 and 1.65 B.M. respectively). However, complex **(2)** shows 5.0 indicating tetragonal axes are present in this complex. Also, the $g_{||}/A_{||}$ values are considered as a diagnostic of stereochemistry [77]. The $g_{||}/A_{||}$ values lie just within the range expected for the complexes Table 4. The orbital reduction factors ($K_{||}$, $K_{\perp}$, K), which are a measure of covalency can be calculated [78]. K Table 4, for the copper(II) complexes **(2)**, **(3)** and **(7)**, indicating covalent bond character [57,79]. The g-values reported here Table 4 show considerable covalent bond character [57,80,81]. Also, the in-plane σ-covalency parameter, α^2(Cu) Table 4 suggests a covalent bonding [49,57,79]. The complexes show show β_1^2 values 0.56, 0.61 and 0.63 indicating a covalency in the in-plane π-bonding [74,79,82]. While ß^2 for complexes **(2)** and **(7)** are 0.46 and 0.58 respectively, indicating covalent bonding character out of-plane π-bonding, however, complex **(3)** shows 1.27, indicating ionic character of the out of-plane [79,82]. The calculated orbital populations (a_d^2) for the copper(II) complexes **(2)**, **(3)** and **(7)**, Table 4, indicate a $d_{(x2-y2)}$ ground state [83,84]. Cobalt(II) complex **(9)** and manganese(II) complex **(10)** show isotropic spectra with values 2.09 and 12.12, respectively indicating octahedral structures [54,73].

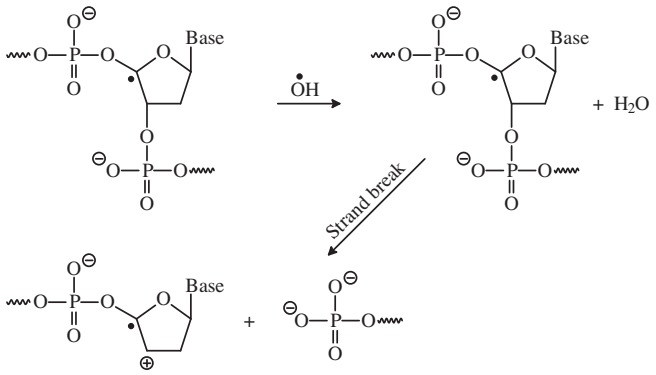

Scheme 1.

Table 6
Mass spectra of **(1)** and its Zn(II) complex **(11)**.

m/z	Rel. Int.	Fragment
70	50	C_3H_4NO
83	55	C_3HNO_2
86	65	$C_3H_4NO_2$
130	25	$C_4H_8N_3O_2$
168	100	$C_{10}H_4N_2O$
189	70	$C_{10}H_9N_2O_2$
203	68	$C_{10}H_9N_3O_2$
216	85	$C_{11}H_{10}N_3O_2$
240	86	$C_{13}H_{10}N_3O_2$
277	70	$C_{14}H_{11}N_3O_2$
309	100	$C_{18}H_{19}N_3O_2$
*Mass spectra of Zn(II) complex **(11)***		
76	50	C_6H_4
104	70	C_7H_5O
148	22	$C_7H_4N_2O_2$
214	21	$C_7H_5N_2O_2Zn$
318	18	$C_{14}H_{11}N_3O_2Zn$
433	15	$C_{20}H_{22}N_3O_2Zn$

Thermal analyses (DTA and TGA)

The thermal curves in the temperature 27–800 °C range for complexes **(3)**, **(6)**, **(7)**, **(9)** and **(11)** are thermally stable up to

Standard drug	Complex **(2)**	complex **(11)**	Complex **(14)**	Complex **(16)**	Complex **(20)**
26.21	23.78	33.56	29.28	40.56	18.62

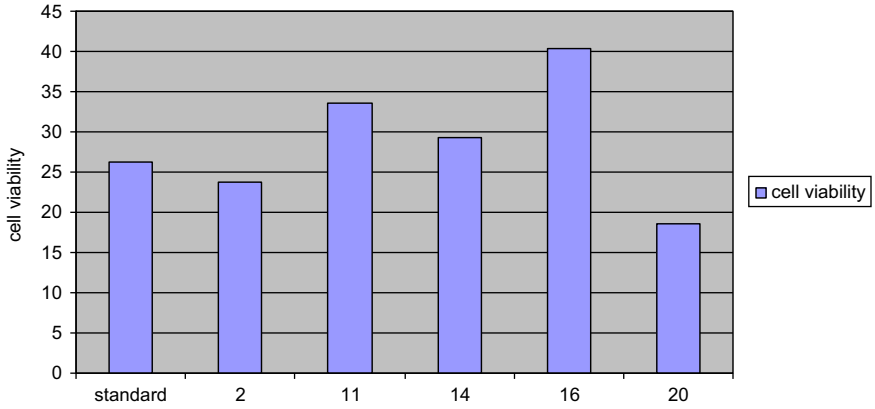

Fig. 2. Antiproliferative effect of **(2)**, **(11)**, **(14)**, **(16)** and **(20)** against HEPG-2 liver cell line (50) μg/ml.

Standard drug	Complex **(2)**	Complex **(11)**	Complex **(14)**	Complex **(16)**	Complex **(20)**
18.89	35.85	54.2	47.9	53.24	31.4

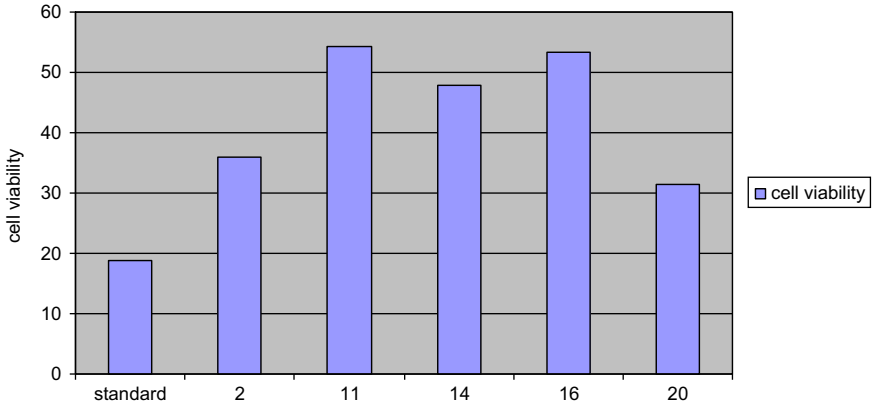

Fig. 3. Antiproliferative effect of **(2)**, **(11)**, **(14)**, **(16)** and **(20)** against HEPG-2 liver cell line at (25) μg/ml.

Standard drug	Complex **(2)**	Complex **(11)**	Complex **(14)**	Complex **(16)**	Complex **(20)**
21.19	43.22	68.58	59.12	70.48	42.58

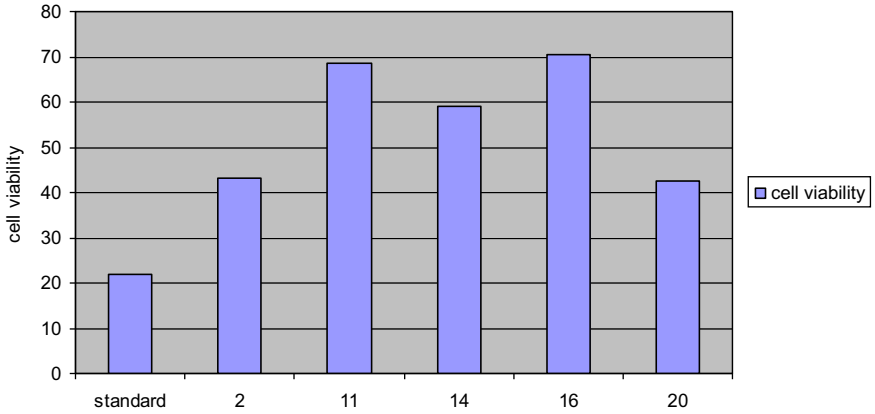

Fig. 4. Antiproliferative effect of **(2)**, **(11)**, **(14)**, **(16)** and **(20)** against HEPG-2 liver cell line at (12.5) μg/ml.

Standard drug	Complex **(2)**	Complex **(11)**	Complex **(14)**	Complex **(16)**	Complex **(20)**
31.18	58.56	81.6	68.24	81.16	53.92

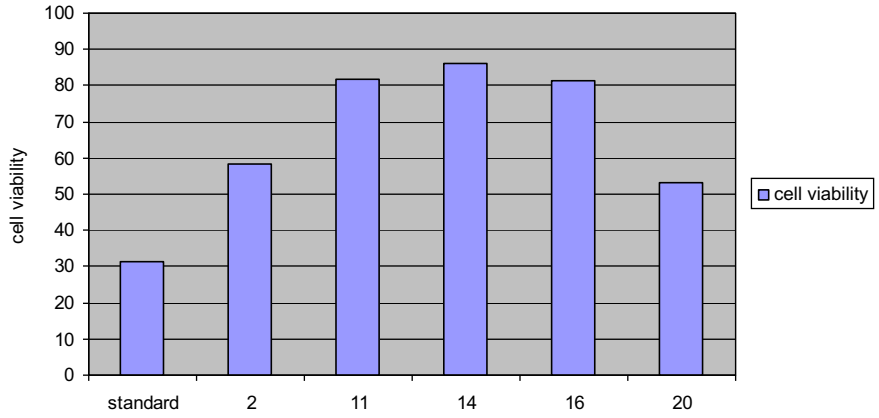

Fig. 5. Antiproliferative effect of compound **(2)**, **(11)**, **(14)**, **(16)** and **(20)** against HEPG-2 liver cell line at (6.25) μg/ml.

Standard drug	Complex **(2)**	Complex **(11)**	Complex **(14)**	Complex **(16)**	Complex **(20)**
73.12	79.7	90.66	79.36	96.22	62.14

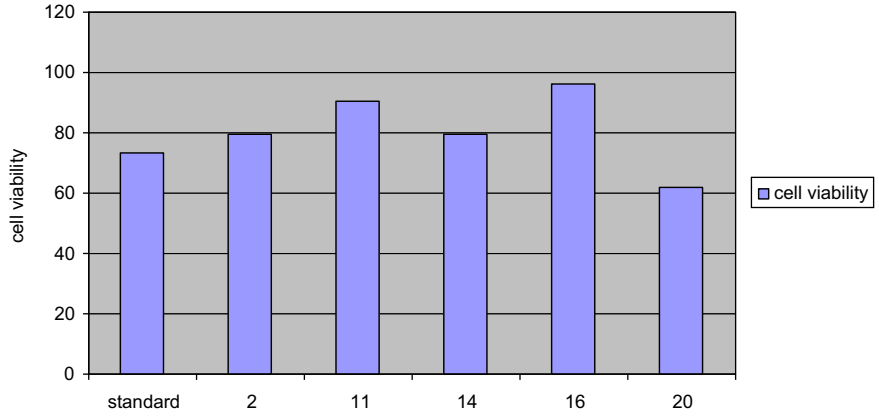

Fig. 6. Antiproliferative effect of compounds **(2)**, **(11)**, **(14)**, **(16)** and **(20)** against HEPG-2 liver cell line at (3.125) μg/ml.

Standard drug	Complex **(2)**	Complex **(11)**	Complex **(14)**	Complex **(16)**	Complex **(20)**
88.5	91.48	98.78	81.2	100	73.25

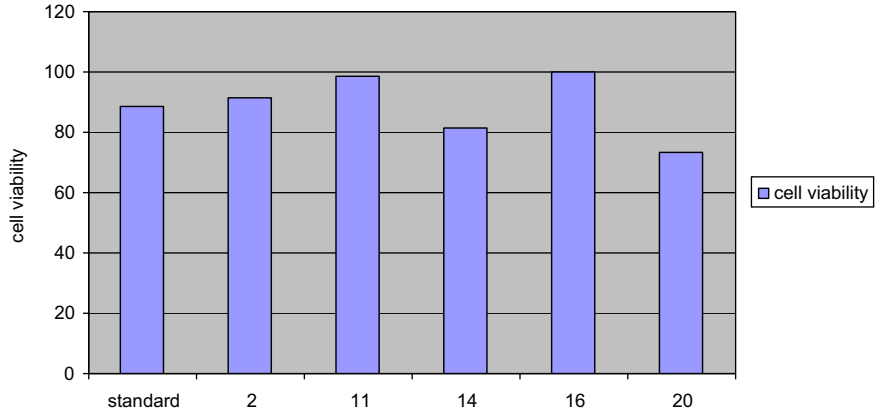

Fig. 7. Antiproliferative effect of compounds **(2)**, **(11)**, **(14)**, **(16)** and **(20)** against HEPG-2 liver cell line at (1.56) μg/ml.

50 °C. Complexes show decomposition step within temperature 60–80 °C range, is due to elimination of hydrated water [85,86] ($3H_2O$, **(3)**, $2H_2O$, **(6)**, $3H_2O$, **(7)**, $2H_2O$, **(9)** and $3H_2O$, **(11)**). Another thermal decomposition within 120–170 °C range, is due to loss of coordinated water ($4H_2O$, **(3)**, $3H_2O$, **(6)**, $3H_2O$, **(7)**, $3H_2O$, **(9)** and $3H_2O$, **(11)**). The complex **(3)** shows one endothermic peak at 255 °C, corresponding to the loss of one terminal coordinated acetate group. Another endothermic peak observed at 285 °C, corresponds to loss of two bridge coordinated acetate group. Endothermic peak observed at 365 °C may be due to melting point. Finally, the complex shows exothermic peaks at 465, 515, 595 and 660 °C corresponding to oxidative thermal decomposition which proceeds slowly with final residue at 660 °C, assigned to CuO [85]. Complex **(6)** shows endothermic peak at 250 °C is due to loss of chloride anion. The endothermic peak observed at 325 °C may be assigned to the melting point. Oxidative thermal decomposition occurs at 365, 390, 430, 500 and 570 °C with exothermic peaks, leaving CuO. Complex **(7)** shows endothermic peak at 255 °C is due to loss of one NO_3 group. The endothermic peak observed at 330 °C may be due to melting point. Oxidative thermal decomposition occurs at 360, 445, 500, 540 and 615 °C with exothermic peaks, leaving CuO [87]. Complex **(9)** shows endothermic peak at 220 °C is due to loss of one sulfate group. The endothermic peak appears at 257 °C is assigned to the loss of two C_7H_7 moiety. Also, another endothermic peak observed at 316 °C is due to melting point. Oxidative thermal decomposition occurs at 400, 480 and 595 °C with exothermic peaks, leaving CoO. Finally, complex **(11)** shows endothermic peak at 294 °C is due to loss of acetate group. At 332 °C, endothermic peak appears which is due to melting point. Oxidative thermal decomposition occurs at 416, 550 and 600 °C with exothermic peaks, leaving ZnO [87]**.** The thermal data are present in Table 5.

Antiproliferative studies

The antiproliferative effects of the ligand, (**1**) and its complexes **(2)**, **(11)**, **(14)**, **(16)** and **(20)** in DMSO were evaluated against HEPG-2 cell line. These were tested by comparing them with the standard drug (Sorafenib). The solvent DMSO showed no effect on cell growth as it reported previously [88]. The ligand **(1)**, showed a weak inhibition effect at ranges of concentration used, however, the complexes showed moderate effect against HEPG-2 cell line.There was a positive correlation between the surviving fraction ratio of HEPG-2 tumor cell line and the concentration. Also, the Cd(II) complex **(20)** showed a high potency of inhibition (65%) at 25 μg/ml against HEPG-2 cell line, compared with a standard drug [87]. This could be explained as follow Cd(II) could bind to DNA where it seemed that, change the anion and the nature of the metal ion in complexes may have effect on the biological behavior, by altering the binding ability of DNA [88–92]. Moreover, Gaetke and Chow had reported that, metal has been suggested to facilitate oxidated tissue injury through a free-radical mediated pathway analogous to the Fenton reaction [93]. By applying the ESR-trapping technique, evidence for metal-mediated hydroxyl radical formation invivo has been obtained [79]. Radicals are produced through a Fenton-type reaction as follows [93]:

$$LM(II) + H_2O_2 \rightarrow LM(I) + {\cdot}OOH + H^+$$

$$LM(I) + H_2O_2 \rightarrow LM(II) + {\cdot}OH + OH^-$$

where L is the ligand.

Also, metal could act as a double-edged, sword by inducing DNA damage and also by inhibiting their repair [94]. The OH radicals react with DNA sugars and bases and the most significant and well-characterized of the OH reactions is hydrogen atom abstraction from the C_4 atom to yield sugar radicals with subsequent β-elimination. Scheme 1, by this mechanism strand breakage occurs as well as the release of the free bases. Another form of attack on the DNA bases is by solvated electrons, probably via a similar reaction to those discussed below for the direct effects of radiation on DNA [81] (Scheme 1).

Table 7

The concentration	Order of antiproliferative effect of the studied complexes
At concentration 50 μg/ml	Cd(II) complex (20) > Cu(II) complex (2) > Standard > Tl(I) complex (14) > Zn(II) complex (11) > Cr(III) complex (16)
At concentration 25 μg/ml	Standard > Cd(II) complex (20) > Cu(II) complex (2) > Tl(I) complex (14) > Cr(III) complex (16) > Zn(II) complex (11)
At concentration 12.5 μg/ml	Standard > Cd(II) complex (20) > Cu(II) complex (2) > Tl(I) complex (14) > Zn(II) complex (11) > Cr(III) complex (16)
At concentration 6.25 μg/ml	Standard > Cd(II) complex (20) > Cu(II) complex (2) > Tl(I) complex (14) > Cr(III) complex (16) > Zn(II) complex (11)
At concentration 3.125 μg/ml	Cd(II) complex (20) > Standard > Tl(I) complex (14) > Cu(II) complex (2) > Zn(II) complex (11) > Cr(III) complex (16)
At concentration 1.56 μg/ml	Cd(II) complex (20) > Tl(I) complex (14) > Standard > Cu(II) complex (2) > Zn(II) complex (11) > Cr(III) complex (16)

The relation between the concentration of the complexes in DMSO and their antiproliferative activity shown in Table 7 and Figs. 2–7. Although, complexes were octahedral structures and had the same anions, the variable activity of the complexes might be due to their oxidation–reduction potentials.

Conclusion

Cr(III), Mn(II), Fe(III), Co(II), Ni(II), Cu(II), Zn(II), Cd(II), Sr(II), Hg(II), Tl(I), UO_2(II) and ZrO(II) complexes of (3E)-2-(hydroxyimino)-N-P-Tolyl-3-(P-tolylimino) butanamide have been prepared and spectrally characterized. The IR data show that, the ligand behaves as monobasic bidentate or neutral bidentate**.** Molar conductances in DMF indicate that, the complexes are non-electrolytes. ESR spectra of solid Cu(II) complexes at room temperature show axial type (d_{x2-y2}) with covalent bond character in an octahedral environment. Complexes showed inhibitory activity against hepatocellular carcinoma (HepG-2 cell line).

References

[1] A. Colak, U. Terzi, M. Col, S.A. Karaoglu, S. Karabocek, A. Kucukdumlu, F.A. Ayaz, Eur. J. Med. Chem. 45 (2010) 5169–5175.
[2] A.S. El-Tabl, W. Plass, A. Buchholz, M.M.E. Shakdofa, J. Chem. Res. (2009) 582.
[3] A. Yilmaz, B. Taner, P. Deveci, A.Y. Obali, U. Arslan, E. Sahin, H.I. Ucan, E. Ozcan, Polyhedron 29 (2010) 2991–2998.
[4] M.I. El-Gamal, S.M. Bayomi, S.M. El-Ashry, S.A. Said, A.A.M. Abdel-Aziz, N.I. Abdel-Aziz, Eur. J. Med. Chem. 45 (2010) 1403–1414.
[5] N.M. Krstie, M.S. Bjelakovie, Z. Zizak, M.D. Pavlovic, V.D. Juranic, Steroids 72 (2007) 406–414.
[6] H.J. Park, K. Lee, S.J. Park, B. Ahn, J.C. Lee, H.J. Cho, K.I. Lee, Bioorg. Med. Chem. Lett. 15 (2005) 3307–3312.
[7] N.I. Dodof, M. Kubiak, J. Kuduk-Jaworska, A. Mastalarz, A. Kochel, V. Vassilievia, N. Vassilev, N. Trendaflova, I. Georgieva, M. Lalia-Kantouri, M. Apostolova, Chemija 20 (2009) 208.
[8] T.W. Thomas, A.E. Underhill, Chem. Soc. Rev. 1 (1972) 99.
[9] K. Oguchi, K. Sanui, N. Ogata, Polym. Eng. Sci. 30 (1990) 449–452.
[10] R.C. Maurya, R. Verma, D. Sutradhar, Synth. React. Inorg. Met-Org. Chem. 33 (2003) 435.
[11] M. Kandaz, I. Yilmaz, S. Keskin, A. Koca, Polyhedron 21 (2002) 825–834.
[12] K.C. Dash, J. Indian Chem. Soc. 71 (1994) 227–238.
[13] V.Y. Kukushkin, D. Tudela, A. Pombeiro, J. Coord. Chem. Rev. 114 (1992) 169.
[14] A.O. Baghlaf, M.M. Aly, N.S. Ganji, Polyhedron 6 (1987) 205–209.
[15] E. Coacio, J.M. Dominguezvera, A. Escuer, M. Klinga, R. Kivekas, A. Romerosa, J. Chem. Soc. Dalton Trans. (1995) 343–348.

[16] R. Ruiz, J. Sanz, F. Lloret, M. Julve, J. Faus, C. Bios, M. Munoz, J. Chem. Soc. Dalton Trans. (1993) 3035.
[17] M.M. Aly, J. Coord. Chem. 43 (1998) 89–113.
[18] M.S. Ray, A. Ghosh, S. Chaudhuri, M.C.B. Drew, I. Ribas, Eur. J. Inorg. Chem. 15 (2004) 3110.
[19] S. Chattopadhay, M.S. Ray, S. Chaudhuri, G. Mukhopahyay, G. Bocelli, A. Cantoni, A. Ghosh, Inorg. Chem. Acta 359 (2006) 1367–1375.
[20] D. Maity, S. Chattopadhyay, A. Ghosh, M.G.B. Drew, G. Mukhopadhyay, Polyhedron 28 (2009) 812–818.
[21] A.S. El-Tabl, Transition Met. Chem. 22 (1997) 400–405.
[22] J. Peisach, W.E. Blumberg, in: T.F. Yen (Ed.), Electron Spin Resonance of Metal Complexes, vol. 71, Plenum Press, New York, 1969.
[23] A.I. Vogel, A Text Book of Quantitative Inorganic Analysis, Longman Suffolk, 1961.
[24] J. Lewis, R.G. Wilkins, Modern Coordination Chemistry, vol. 40, Interscience, New York, 1960. pp. 403–406.
[25] P. Skehan, R. Storeng, et al., J. Natl. Cancer Inst. 82 (1990) 1107.
[26] W. Geary, J. Coord. Chem. Rev. 7 (1971) 81–122.
[27] A.S. El-Tabl, F.A. El-Said, A.N. Al-Hakim, W. Plass, Trans. Met. Chem. 67 (2007) 265.
[28] H. Kantekin, U. Ocak, Y. Gok, H. Alp, J. Coord. Chem. 57 (2004) 265.
[29] W. Plass, A.S. El-Tabl, A. Pohlman, Coord. Chem. 62 (2009) 358–372.
[30] R. Gup, E. Giziroglu, Spectrochim Acta: Part A 65 (2006) 719–726.
[31] E. Tas, M. Aslanoglu, A. Kilic, Z. Kara, Trans. Met. Chem. 30 (2005) 758–764.
[32] K.B. Gudasi, M.S. Patil, R.S. Vadavi, R.V. Shenoy, S.A. Patil, M. Nethayi, Trans. Met. Chem. 31 (2006) 580–585.
[33] S. El-Tabl, R.M. El-Bahnasawy, M.M.E. Shakdofa, E. El-Deen Abdalah, J. Chem. Reas. 88 (2010).
[34] R.S. Baligar, V.K. Revankar, J. Serb. Chem. Sac. 71 (2006) 1301.
[35] C. Dongli, J. Handong, Z. Hongyum, M.C. Degi, Y. Jina, L.B. Jian, Polyhedron 13 (1994) 57.
[36] E. Tas, A. Cukuroval, J. Coord. Chem. 47 (1999) 425.
[37] M. El-Behry, M. El-Twigry, Spectrochim Acta: Part A 66 (2007) 28.
[38] F. Brezina, Z. Smekal, Z. Sindelar, R. Pastorek, J. Mrozinski, Trans. Met. Chem. 21 (1996) 287.
[39] K. Nakatamato, Infrared Spectra of Inorganic and Coordination Compounds, second ed., Wiley Inc., New York, 1967.
[40] A.S. El-Tabl, Trans. Met. Chem. 27 (2002) 166–170.
[41] B.B. Mahapatra, B.K. Mahapatra, J. Inorg. Nucl. Chem. 39 (1997) 2291.
[42] A.S. El-Tabl, Ph.D. Thesis, Menoufia University, Egypt, 1993.
[43] O. Pouralimardan, A.C. Chamayou, C. Janiak, H. Hosseini-Monfared, Inorg. Chem. Acta 360 (2007) 1599–1608.
[44] M.M. Aly, A.O. Baghlaf, N.S. Ganji, Polyhedron 4 (1985) 1301–1309.
[45] A.S. El-Tabl, K. El-Baradie, R.M. Issa, J. Coord. Chem. 56 (2003) 1113.
[46] W.H. Hegazy, Monatsch. Chem. 132 (2001) 639–654.
[47] A.S. El-Tabl, J. Chem. Res. (2002) 529–531.
[48] M.F.R. Fouda, M.M. Abd-El-Zaher, M.M. Shakdofa, F.A. El-Sayed, M.I. Ayad, A.S. El-Tabl, J. Coord. Chem. 61 (2008) 1983.
[49] H.A. Kuska, M.T. Rogers, Coordination Chemistry Martell AE Ed, vol. 92, Van Nostrad Reihoid Co., New York, 1971.
[50] R.M. El-Bahnasawy, A.S. El-Tabl, E. El-Sheroafy, T.I. Kashar, Y.M. Issa, Polish J. Chem. 73 (1995).
[51] A.S. El-Tabl, R.M. Issa, M.A. Morsi, Trans. Met. Chem. 57 (2004) 265–282.
[52] S.K. Nakamoto, Infrared and Raman spectra of Inorganic and Coordination Compounds, third ed., John Wiley & Sons, New York, 1977. pp. 244–247.
[53] R.A. Lai, A. Kumar, Ind. J. Chem. 38A (1999) 839.
[54] N. Raman, Y. Pitchaikani, A. Kulandaisamy, Proc. Indian Acta (Chem. Sci.) 133 (2001) 183.
[55] K.B. Gudasi, S.A. Patel, R.S. Vadvavi, R.V. Shenoy, M. Nethayi, Trans. Met. Chem. 31 (2006) 586.
[56] A.E. Motaleb, M. Ramadan, W. Sawodny, H. Baradie, M. Gaber, Trans. Met. Chem. 22 (1997) 211–215.
[57] A.N. Al-Hakimi, M.M.E. Shakdofa, A.M.A. El-Saidy, A.S. El-Tabl, J. Kor. Chem. Soc. 55 (2011) 418.
[58] F. Sabin, A. Vogler, Monta Chem. 123 (1992) 705–710.
[59] K.B. Gudasi, S.A. Patil, R.S. Rashmi, V. Shenoy, M. Nethaji, Trans. Met. Chem. 31 (2006) 580.
[60] A.S. El-Tabl, S.A. El-Enein, J. Coord. Chem. 57 (2004) 281.
[61] E.W. Ainscough, A.M. Brodie, A.J. Dobbs, J.D. Ranford, J.M. Waters, Inorg. Chem. Acta 267 (1998) 27–38.
[62] S.A. Sallam, A.S. Orabi, B.A. El-Shetary, A. Lentz, Trans. Met. Chem. 27 (2002) 447.
[63] N.V. Takkar, S.Z. Bootwala, Indian J. Chem. 34A (1995) 370–374.
[64] G.C. Chinvmia, D.G. Phillips, A.D. Rae, Inorg. Chim. Acta 238 (1995) 197–201.
[65] B.H. Krishna, C.M. Mahapatra, K.C. Dush, J. Inorg. Nucl. Chem. 39 (1997) 1253.
[66] R.K. Parihari, R.K. Patel, R.N. Patel, J. Ind. Chem. Soc. 77 (2000) 339.
[67] F. Sabin, A. Vogler, Monta Chem. 123 (1992) 705–708.
[68] A.S. El-Tabl, F.A. El-Saied, A.N. Al-Hakimi, J. Coord. Chem. 61 (2008) 2380–2401.
[69] N.K. Singh, S.B. Singh, Trans. Met. Chem. 26 (2001) 487–495.
[70] G.M. Abu El-Reash, K.M. Ibrahim, M.M. Bekheit, Trans. Met. Chem. 15 (1990) 148.
[71] A.B.P. Lever, Inorganic Electronic Spectroscopy, Elsevier Pub Company, New York, 1968. pp. 275–283.
[72] A.S. El-Tabl, Bull. Korean Chem. Soc. 25 (2004) 1–6.
[73] A.S. El-Tabl, M.M.E. Shakdofa, A.M.A. El-Seidy, Korean J. Chem. Soc. 55 (2011) 603.
[74] H.A. El-Boraey, A.S. El-Tabl, Polish J. Chem. 77 (2003) 1759–1775.
[75] A.S. El-Tabl, Trans. Met. Chem. 23 (1998) 63.
[76] I.M. Procter, B.J. Hathaway, P.N. Nicholls, J. Chem. Soc. A (1969) 1678–1684.
[77] D.E. Nickless, M.J. Power, F.L. Urbach, Inorg. Chem. 22 (1983) 3210–3217.
[78] R.K. Ray, Inorg. Chim. Acta 174 (1990) 257.
[79] A.S. El-Tabl, J. Chem. Res. (2004) 19.
[80] D. Kivelson, R. Neiman, J. Chem. Phys. 35 (1961) 149–155.
[81] D.W. Smith, J. Chem. Soc. A (1971) 3108–3120.
[82] M.M. Bhadbhade, D. Srinivas, Inorg. Chem. 32 (1993) 2458.
[83] M.C.R. Symons, Chemical and Biological Aspects of Electron Spin Resonance, Van Nostrand Reinhold, Wokingham, 1979.
[84] A.S. El-Tabl, J. Chem. Res. 22 (2002) 595–632.
[85] A.S. El-Tabl, S.M. Imam, Trans. Met. Chem. 22 (1997) 259.
[86] M. Gaber, M.M. Ayad, Thermochim. Acta 176 (1991) 21–29.
[87] A.S. El-Tabl, M.M. Abou-Sekkina, Polish J. Chem. 73 (1999) 1937–1945.
[88] N.A. Illan-Cabeza, A.R. Garcia-Garcia, M.N. Moreno-carretero, J.M. Martinez-Martos, M.I. Ramirez-exposito, J. Inorg. Biochem. 99 (2005) 1637–1645.
[89] I.H. Hall, C.C. Lee, G. Ibrahim, M.A. Khan, G.M. Bouet, Appl. Organomet. Chem. 11 (1997) 565–575.
[90] G. Feng, J.C. Mareque-Rivas, R.T. Rosales, N.H. Williams, J. Am. Chem. Soc. 127 (2005) 13470–13471.
[91] J.C. Mareque, R. Prabaharan, S. Parsons, Dalton Trans. 21 (2004) 1648–1655.
[92] B. Bauer-Siebenlist, F. Meyer, E. Farkas, D. Vidovic, S. Dechert, J. Chem. Eur. 11 (2005) 4349–4360.
[93] L.M. Gaetke, C.K. Chow, Toxicology 189 (2003) 147–163.
[94] C.A. Rouzer, Chem. Res. Toxicol. 23 (2010) 1517–1518.